Magnetic frustration and iron-vacancy ordering in iron chalcogenide

Chen Fang,[1,*] Bao Xu,[2] Pengcheng Dai,[2,3] Tao Xiang,[2,4] and Jiangping Hu[1,2]

[1]*Department of Physics, Purdue University, West Lafayette, Indiana 47907, USA*

[2]*Beijing National Laboratory for Condensed Matter Physics, Institute of Physics, Chinese Academy of Sciences, Beijing 100080, China*

[3]*The University of Tennessee, Knoxville, Tennessee 37996-1200, USA*

[4]*Institute of Theoretical Physics, Chinese Academy of Sciences, Beijing 100080, China*

(Received 11 April 2011; revised manuscript received 28 January 2012; published 2 April 2012)

We study the spin- and vacancy-ordered states in 122 iron chalcogenides ($A_{1-y}Fe_{2-x}Se_2$) by inspecting the magnetic ground states of a J_1-J_2-J_3 model on different vacancy-ordered lattices observed/conjectured in these compounds. A highly frustrated J_1-J_2-J_3 model was first applied to the study of magnetism in FeTe and was reported to explain the inelastic neutron-scattering data qualitatively. We find that the vacancy-ordered states are generally energetically favored for their reduction of magnetic frustration inherent to the spin-exchange model and, especially, that the 245 vacancy-spin-ordered state minimizes the magnetic exchange energy among all known vacancy-ordered states, in line with the fact that it has the highest vacancy-ordering phase transition temperature and the largest ordered moment in all iron-based superconductors. Thus, our study provides an electronic perspective for understanding the various vacancy orderings in these compounds. Then we focus on the experimentally well-studied 245 state and calculate the spin-wave spectrum and dynamic spin susceptibility. Finding that the key features of these calculated quantities are consistent with a recent inelastic neutron-scattering experiment, we conclude that we have obtained a qualitative local spin model for the 245 state. We also discuss the possibility of a unified local-moment description for all iron chalcogenides based on our result.

DOI: 10.1103/PhysRevB.85.134406 PACS number(s): 75.30.−m, 75.30.Ds

I. INTRODUCTION

The recent discovery of a new family of iron-based superconductors, the 122 iron chalcogenides A(K,Cs,Rb)$_y$Fe$_{2-x}$Se$_2$,[1–3] with a superconducting (SC) transition temperature even higher than 40 K, has attracted much research attention. The compounds are heavily electron doped with only electron Fermi pockets, mainly located at the M point of the folded Brillouin zone (BZ) shown by both angle-resolved photoemission spectroscopy[4–6] and local-density approximation (LDA) calculations.[7–9]

Although almost all compounds of the family share key features in electronic structures, it is difficult to make a general statement on the vacancy ordering and spin ordering in $A_{1-y}Fe_{2-x}Se_2$, as the type of vacancy order and magnetic order is highly sensitive to the contents (x and y) of the specific compound. Furthermore, it is technically very hard to prepare a single-phase sample, rendering the assignment of a specific ordering to a specific compound practically impossible. Currently, people are only convinced that iron vacancies always populate all compounds of the family and they can order into different patterns in different compounds and at various temperatures.[10,12–16] Experiments show signs of possible magnetic ordering at temperatures below or very close to the vacancy-ordering temperatures, and first-principle calculations propose various spin-ordering configurations for various vacancy patterns; however, the only experimentally established magnetic order is the "block antiferromagnetism" in the 245 compounds (named after their nominal stoichiometric formula $A_2Fe_4Se_5$, obtained by taking $x = 0.2$ and $y = 0.4$). The magnetic ordering temperature can be as high as 500 K and the ordered moment can be as large as three Bohr magnetons,[10,11] both of which make new records in all iron-based superconductors. These interesting yet peculiar properties warrant a focused study on the link between vacancy patterns and magnetism in these systems.

For iron pnictides, their parental compounds display a universal collinear antiferromagnetic (CAFM) phase,[17] which can be described by a simple magnetic exchange model including the nearest neighbor (NN) spin exchange J_1 (becoming J_{1a} and J_{1b} due to rotation symmetry breaking in the orthorhombic phase) and the next-nearest neighbor (NNN) spin exchange J_2.[18,19] However, for iron chalcogenides, different magnetic orders have been observed.[20,21] For example, the 11 iron chalcogenides, FeTe$_{1-x}$Se$_x$,[22] which can achieve the superconducting transition temperature around 40 K under pressure,[23] can display both commensurate and incommensurate magnetic states. The ordered magnetic moment of the parent compound FeTe is about $2.0\mu_b$, significantly larger than iron pnictides as well. Recently, it has been shown that the magnetic state of FeTe, a bicollinear antiferromagnet (BAFM), can be described by a strongly frustrated magnetic model including the nearest neighbor J_1, the next-nearest neighbor J_2, and the third-nearest neighbor (TNN) J_3, i.e., the J_1-J_2-J_3 model.[24,25] It has been determined that J_1 is ferromagnetic (FM) while J_2 and J_3 are antiferromagnetic (AFM).[26]

The values of the magnetic exchange coupling parameters suggest that FeTe is close to a boundary between an incommensurate magnetic phase and the BAFM phase so that the latter can easily be destabilized by an introduction of a small percentage of additional Fe atoms.[20]

However, it is still debated whether the effective models with local magnetic exchange couplings are the right models for describing the magnetism in iron-based superconductors. For iron pnictides, there is less debate since the model is simple and has gained support from different families of iron pnictides. However, for iron chalcogenides, the model lacks independent verification. Since the local physics of the 122

iron chalcogenides should be similar to the one of FeTe, it is naturally expected that both families of iron chalcogenides should be described by similar models.

In this paper, we show that the theories for magnetism in both families of iron chalcogenides can be unified under the J_1-J_2-J_3 model obtained for FeTe, where J_1 is ferromagnetic and $J_{2,3}$ antiferromagnetic. On one hand, we show that the magnetic frustration in the J_1-J_2-J_3 model is reduced when there is vacancy ordering and that, among various vacancy-ordering patterns, the 245 state maximizes this reduction and is hence energetically most favorable. The reduced frustration in the 245 state compared with the high frustration in vacancy-free FeTe is also reflected in the high Neel transition temperature of the 245 state. These findings point to a possible magnetic origin of the vacancy ordering. On the other hand, we calculate spin-wave excitations over the 245 magnetic ground state and identify features characteristic of the J_1-J_2-J_3 model. These features are confirmed in a recent inelastic neutron-scattering experiment on $Rb_{0.8}Fe_{1.58}Se2$, a typical sample having the 245 state as the ground state. This shows that the J_1-J_2-J_3 model is qualitatively relevant to the magnetism of the 245 state, as it is to the magnetism of FeTe.

The paper is organized as follows. In Sec. II we calculate the classical ground-state energies of the J_1-J_2-J_3 model given a few vacancy patterns predicted by previous first-principle calculation and supported by x-ray diffraction. Using parameters ($J_{1,2,3}$) from a recent fitting, the 245 state is found to save the largest amount of exchange energy per site, compared with other vacancy patterns. In Sec. III we calculate the spin-wave excitations for the 245 state and the local dynamic susceptibility. Three sets of parameters are chosen as representatives of three possible parameter regions, and for each set we go through features of the spin-wave spectrum. In Sec. IV, we discuss other factors that may contribute to the vacancy ordering but are not considered in the current model, and we compare our model and result with those of earlier first-principle calculations. We also discuss the implications of the J_1-J_2-J_3 spin model on the superconductivity in iron chalcogenides. We briefly summarize the work in Sec. V.

II. MAGNETIC FRUSTRATION REDUCED BY VACANCIES IN THE 245 STATE

Before we start to consider the effect of vacancy, let us review the J_1-J_2-J_3 model, which was used to describe the magnetism in FeTe.[24,25] The Hamiltonian is given by

$$H = \sum_{\alpha} J_{\alpha} \sum_{\langle ij \rangle_{\alpha}} S_i \cdot S_j \qquad (1)$$

where $\alpha = 1,2,3$ and $\langle\rangle_{1,2,3}$ is the first, second, and third neighbor, respectively. The BAFM state in FeTe, which breaks the rotation symmetry, is stabilized by a coupling to the small lattice distortion. In the BAFM state, this broken symmetry can generate the anisotropy in J_1 (J_{1a} and J_{1b}) and J_2 (J_{2a} and J_{2b}) couplings. For FeTe, by fitting the spin-wave spectrum, we have obtained the values of the magnetic exchange couplings with $J_1 S \sim -34$ meV, $J_2 S \sim 22$ meV, and $J_3 S \sim 7$ meV,[26] where S is the spin of each site. The anisotropy is shown mainly in J_1, with $\frac{J_{1a}-J_{1b}}{2} \sim -16$ meV.[26] The most important

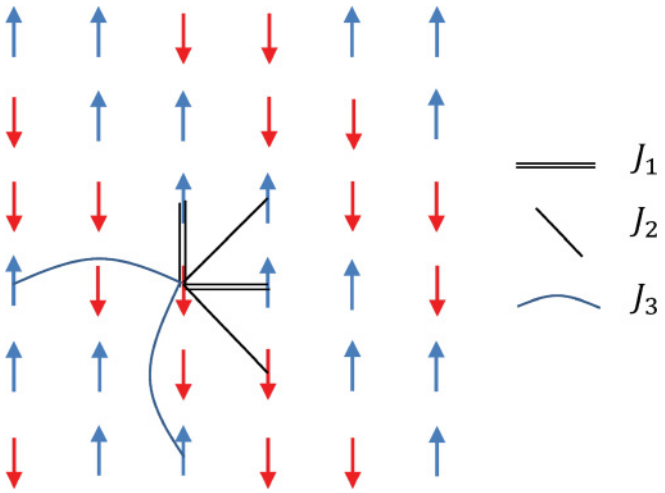

FIG. 1. (Color online) The bicollinear antiferromagnetic spin structure of Fe spins observed in the 11 (FeTe/Se) systems. The figure does not reflect a small lattice distortion in the magnetic phase. The distortion can be viewed as an elongation of the unit cell along the diagonal direction, which is 45 deg away from the lattice distortion observed in iron pnictides. From the figure, it is easy to see that in this ground state J_1 and J_2 are highly frustrated.

feature revealed from the fitting is that the NN coupling J_1 is FM while the other two, J_2 and J_3, are AFM. The sum of these three coupling parameters is close to zero, which indicates the model is highly magnetically frustrated.

Let us first ignore the anisotropy of the magnetic exchange coupling $J_{1,2}$ caused by symmetry breaking in the BAFM state. We focus on the magnetic model in the tetragonal square lattice. In the BAFM state as shown in Fig. 1, both J_1 and J_2 are frustrated couplings and the magnetic energy is only saved by J_3. The saved magnetic energy per site is given by $E_{\mathrm{BAFM}} = -2J_3S^2$.

Now turn to the system of interest. Sharing with FeTe the same structure and components of the FeSe plane, stoichiometric (vacancy-free) 122 chalcogenides are expected to be described by a similar J_1-J_2-J_3 model with parameters qualitatively consistent with those in FeTe, because we have assumed a local-moment picture. To this "parent model," we add vacancies in ordered patterns as observed or predicted in $A_xFe_{2-y}Se_2$. Around one vacancy, J_1's, J_2's, and J_3's connecting to it are removed, and J_3 couplings that have the vacancy along the exchange pathway are also removed. The spins will reorder themselves to the change of the model. We will see that the ground-state energy of the adapted model is lower than the parent model; i.e., the magnetic frustration is reduced by the vacancy ordering.

First we study the 245 state shown in Fig. 2, the magnetic structure of which has been identified by neutron-scattering experiments.[10] In the 245 vacancy-ordered state, each site has three NN and NNN couplings to its neighbors. Moreover, one spin in every consecutive five spins (a 5-1 pattern) along the Fe-Fe direction is removed. The odd number of links for both NN and NNN couplings reduces the magnetic frustration considerably. The 5-1 pattern saves energy from J_3 as well. Therefore, the 245 state enhances the energy saving from all magnetic exchange couplings. The magnetic energy

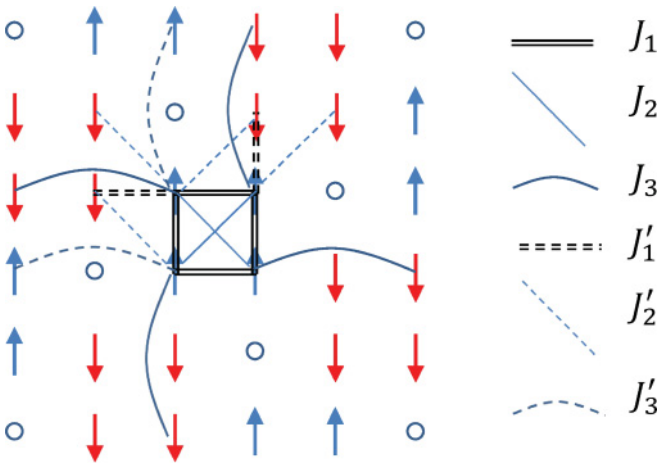

FIG. 2. (Color online) Schematic of the J_1-J_2-J_3 model in the 245 state. J_1 and J_1' are NN couplings when the two spins belong to the same and different four-spin blocks, respectively; J_2 and J_2' are NNN couplings when the two spins belong to the same and different four-spin blocks, respectively; J_3 and J_3' are TNN couplings when the two spins belong to the same and different four-spin blocks, respectively. Couplings not plotted in the figure can be obtained by translating the plotted couplings by the lattice period of the vacancy-ordered phase.

saving per spin $E_{245} = (-J_1 + J_2 + 2J_3)S^2/2$. If we ignore the lattice distortion and use the exchange parameters derived from FeTe, $E_{245} \sim 70S$ meV, compared to $E_{\mathrm{BAFM}} \sim 14S$ meV. Considering the fact that the ordered magnetic moment, $S \sim 3\mu_b$, is also around 1.5 times larger in the 245 state than in FeTe ($S \sim 2\mu_b$), the ratio of the magnetic energy savings between two states is given by $1.5 \times E_{245}/E_{\mathrm{BAFM}} \sim 7.5$. This ratio is in quantitative agreement with the ratio of their magnetic transition temperatures 500 K/70 K ~ 7.1. (Note: In general, the magnetic transition temperature in a quasi-two-dimensional material is given by $T_N \propto \frac{E}{\ln \frac{E}{J_c}}$, where J_c is the coupling strength between layers and E is the in-plane magnetic energy saving. It is almost linear in E if $E \gg J_c$.) This shows that the high transition temperature in the 245 state may be ascribed to the large reduction of magnetic frustration in the J_1-J_2-J_3 model.

It is also interesting to explore other possible vacancy patterns and their associated magnetic orders. For such a frustrated J_1-J_2-J_3 magnetic model, however, there is no other pattern that can reduce the magnetic frustration as significantly as the 245 state. We list some possible patterns:

(1) Armchair dimer crystal patterns (the 212 pattern if we consider K_2FeSe_2) shown in Fig. 3(a). In this pattern, half of the spins are replaced by vacancies. The magnetic energy saving per site is given by $E_{\mathrm{ADC}} = (J_2 - J_1)S^2/2$. The pattern saves energy both from the NN FM and NNN AFM couplings.

(2) Square dimer crystal patterns shown in Fig. 3(b). The energy saving from this structure stems from the NN FM J_1, the NNN AFM J_2, and $E_{\mathrm{SDC}} = \frac{-4J_1+2J_2}{5}S^2$.

(3) The 234 vacancy patterns (named after $K_2Fe_3Se_4$) shown in Figs. 3(c) and 3(d). There are two different patterns. The first pattern saves energy from FM J_1 and AFM J_2 but pays an energy cost for AFM J_3. The energy saving per site is given by $E_{234a} = (-J_1/3 + 2J_2 - 2J_3)S^2$. This magnetic

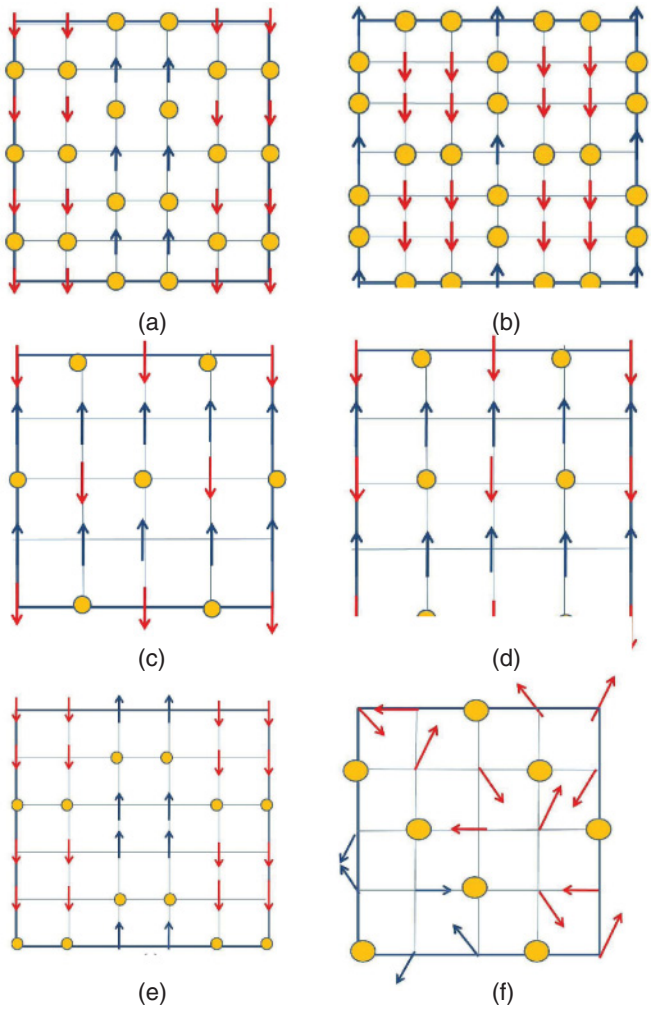

FIG. 3. (Color online) Possible vacancy orderings other than the experimental 245 state and their ground-state spin configurations calculated assuming a J_1-J_2-J_3 model with ferromagnetic J_1. (a) The armchair dimer crystal pattern. (b) The square dimer crystal pattern. These two patterns correspond to $(x = 1, y = 0.5)$ or AFe_2Se_4. (c) and (d) The two different possible vacancy patterns for $(x = 0.5, y = 0)$ or $A_2Fe_3Se_4$. (e) and (f) Two different possible patterns for $A_4Fe_4Se_6$: (e) the dimer vacancy ordering similar to the CAFM magnetic phase and (f) the diagonal stripe pattern where the magnetic ordering is incommensurate.

structure is similar to the $(0,\pi)$ collinear AFM (CAFM) observed in the parental compounds of iron pnictides. In the second pattern, the magnetic state is also similar to CAFM. The energy saving is given by $E_{234b} = \frac{4S^2}{3}(J_2 - J_3/2)$. In general, the 234 phase where the iron concentration is close to 1.5 per unit cell most likely supports a CAFM magnetic phase, similar to iron pnictides. In both patterns, there are ferromagnetic moments on each layer. Between layers, spins are antiferromagnetically aligned. The 234 vacancy pattern has been observed experimentally.[27] However, the magnetic order has not been identified.

(4) The 446 pattern ($K_4Fe_4Se_6$) shown in Figs. 3(e) and 3(f). There are also two possible patterns. The first pattern is a dimer vacancy ordering. The magnetic pattern is also close to the CAFM phase with an energy saving given by

TABLE I. Possible magnetic ground-state configurations with their energies magnetically saved. See Ref. 35 for the parameters chosen for calculating the absolute values in the third column.

Configuration	Energy saved (formula)	Energy saved (meV)
E_{245}	$\frac{-2J_1-J_1'+2J_2'-J_2+2J_3}{2}S^2$	47.5S
E_{212}	$(J_2-J_1)S^2/2$	30S
E_{SCD}	$\frac{-4J_1+2J_2}{5}S^2$	33.6S
E_{234a}	$(-J_1/3+2J_2-2J_3)S^2$	18S
E_{234b}	$\frac{4(J_2-J_3/2)}{3}S^2$	10S
E_{446a}	$\frac{J_2-J_3-3J_1}{4}S^2$	27.75S
E_{446b}	$\frac{3J_2S^2}{2}+\frac{J_1^2S^2}{8J_2}$	31.5S

$E_{234a}=\frac{J_2-J_3-3J_1}{4}S^2$. The second pattern can be viewed as a diagonal stripe similar to undoped cuprates.[28] For such a stripe pattern, all J_3's are removed. The magnetic structure can be predicted to be incommensurate along the stripe direction and AFM along the direction perpendicular to the stripe. The total energy saving per site is given by $E_{446}=\frac{3S^2}{2}J_2+\frac{J_1^2S^2}{8J_2}$. The spin angle between two NN sites along the stripe direction is given by $\cos\theta=-\frac{J_1}{4J_2}$. In Table I, we list the candidates for vacancy ordering and their respective energies given in algebraic expressions and values calculated using the parameters resulted from a fitting to an inelastic neutron experiment.[35]

From the table, we find that all vacancy patterns save magnetic energy in a highly frustrated J_1-J_2-J_3 model, while the 245 state has the largest energy saving. This finding points to a possible electronic origin of the vacancy ordering in these compounds. The ordered vacancies are energetically preferred over the disordered vacancies. For this reason the vacancies will form at least short-ranged orders to save energy. And the 245 vacancy pattern, being the most energetically favored, is more likely to occupy a larger domain.

III. PROPERTIES OF THE 245 STATE IN THE LARGE-*S* LIMIT

The 245 state is clearly the most stable magnetic state in our model. In the following, we focus on this state. In the ordered state, due to the anisotropy introduced by the vacancy orderings, J_1 breaks into J_1 and J_1' and J_2 breaks into J_2 and J_2'. For a general discussion, we recover TNN couplings with a vacancy along the exchange pathway and denote them J_3''s, differentiated from J_3 couplings that have no vacancy along the path. See Fig. 2 for a schematic of this model. First, we analyze the spin excitation in the large-S limit. To start a spin-wave calculation, we denote the spin sites as follows. A generic position of the spin is given by $\mathbf{r}=m\mathbf{l_1}+n\mathbf{l_2}+\mathbf{d_i}$, where m,n are integers and $\mathbf{l_1}=(2\mathbf{x}-\mathbf{y})/\sqrt{5}$,$\mathbf{l_2}=(\mathbf{x}+2\mathbf{y})/\sqrt{5}$, $\mathbf{d_1}=0$, $\mathbf{d_2}=\mathbf{x}$, $\mathbf{d_3}=\mathbf{x}+\mathbf{y}$, $\mathbf{d_4}=\mathbf{y}$, where $\mathbf{x},\mathbf{y}$ are unit vectors in the original orthorhombic lattice. We take the Holstein-Primakoff transform for the given block-AFM ground state:

For $m+n$ even,

$$\begin{aligned} S_+(\mathbf{r})&=\sqrt{2S}a_i(\mathbf{R}),\\ S_-(\mathbf{r})&=\sqrt{2S}a_i^\dagger(\mathbf{R}),\\ S_z(\mathbf{r})&=S-a_i^\dagger(\mathbf{R})a_i(\mathbf{R}). \end{aligned} \tag{2}$$

For $m+n$ odd,

$$\begin{aligned} S_+(\mathbf{r})&=\sqrt{2S}a_i^\dagger(\mathbf{R}),\\ S_-(\mathbf{r})&=\sqrt{2S}a_i(\mathbf{R}),\\ S_z(\mathbf{r})&=-S+a_i^\dagger(\mathbf{R})a_i(\mathbf{R}). \end{aligned} \tag{3}$$

The full Hamiltonian of the model can be put in a matrix form. Define $\psi^\dagger(k)=[a_1^\dagger(k),a_2^\dagger(k),a_3^\dagger(k),a_4^\dagger(k),a_1(-k),a_2(-k),a_3(-k),a_4(-k)]$, and we have

$$H=\frac{1}{2}\sum_k \psi^\dagger(k)\begin{bmatrix}A(k) & B(k)\\ B(k) & A(k)\end{bmatrix}\psi(k). \tag{4}$$

$A(k)$ and $B(k)$ are four-by-four matrices, defined by

$$A(k)=S\begin{pmatrix} E_0 & J_1e^{ik_x} & J_2e^{ik_x+ik_y}+J_3'e^{-i2k_x} & J_1e^{ik_y}\\ . & E_0 & J_1e^{ik_y} & J_2^{-ik_x+ik_y}+J_3'e^{-2ik_y}\\ . & . & E_0 & J_1e^{-ik_x}\\ . & . & . & E_0\end{pmatrix}, \tag{5}$$

$$B(k)=S\begin{pmatrix} 0 & J_2'e^{-ik_x+ik_y}+J_3e^{-2ik_y} & J_1'e^{-ik_y} & J_2'e^{-ik_x-ik_y}+J_3e^{2ik_x}\\ . & 0 & J_2'e^{-ik_x-ik_y}+J_3e^{2ik_x} & J_1'e^{ik_x}\\ . & . & 0 & J_2'e^{ik_x-ik_y}+J_3e^{2ik_y}\\ . & . & . & 0\end{pmatrix}, \tag{6}$$

where $E_0=-2J_1-J_2+J_1'+2J_2'+2J_3-J_3'$. The lower triangle elements are suppressed because both matrices are hermitian.

By diagonalizing this Hamiltonian, we have

$$H=\sum_{i=1,2,3,4;k}[\gamma_i^\dagger(k)\gamma_i(k)+1/2]\omega_i(k) \tag{7}$$

and

$$a_i(k) = \sum_j U_{ij}(k)\gamma_j(k) + V_{ij}(k)\gamma_j^\dagger(-k). \quad (8)$$

where U and V are 4×4 matrices to diagonalize the Hamiltonian. The spin reduction due to quantum fluctuations on each site is given by

$$\delta m = \frac{1}{4\pi^2}\sum_j \int_0^{2\pi} dk_x \int_0^{2\pi} dk_y |V_{1j}(k_x,k_y)|^2. \quad (9)$$

It is also interesting to calculate the dynamic factor $S(\omega) = -\Im[\chi(\omega)]$, where the local susceptibility $\chi(\omega)$ is defined as

$$\chi(i\omega_n) = \sum_q \int d\tau e^{i\omega_n\tau}[\langle S^+(q,\tau)S^-(-q,0)\rangle + \langle S^-(q,\tau)S^+(-q,0)\rangle]/N. \quad (10)$$

After taking the Fourier transform, we obtain (from here, $S = 1$ is assumed for simplicity)

$$\chi(\omega) = \sum_k \sum_{i,j}(|V_{i,j}(k)|^2 + |U_{i,j}(k)|^2) \times \left[\frac{1}{\omega - E_j(k) + i0} + \frac{1}{\omega + E_j(k) + i0}\right]/N. \quad (11)$$

Due to the enlarged unit cell, the BZ is one fifth of the original unfolded BZ for one Fe per unit cell. The BZ is cornered by the four (equivalent) points $(-3\pi/5,-\pi/5)$, $(\pi/5,-3\pi/5)$, $(3\pi/5,\pi/5)$, and $(-\pi/5,3\pi/5)$, and these points are called M_s points. It is convenient to define $X_s = (2\pi/5,-\pi/5)$ and $Y_s = (-\pi/5,-2\pi/5)$ for later discussion.

The spin wave has four branches. Depending on the parameters, there can be finite gaps between the first and the second branches and between the third and the fourth ones. The middle two branches are degenerate at Γ and M_s points and are in general close to each other. At high-symmetry points, the spin-wave energy has analytic expressions. We take $S = 1$ for convenience. At M_s and Γ, $E_1(\Gamma) = 0, E_2(\Gamma) = E_3(\Gamma) = 2\sqrt{(J_e - J_1 - J_2 - J_3')(J_1' - J_1 - J_2 + J_e - J_3')}$, and $E_4(\Gamma) = 2\sqrt{2}\sqrt{(J_1' - 2J_1)(J_e - J_1)}$ where $J_e = J_2' + J_3$ is the effective antiferromagnetic coupling strength between two four-spin plaquettes. At X_s, $E_1(X_s) = 2[J_1 + \sqrt{(J_e - J_3' - J_1)(J_1' + J_e - J_3' - J_1)}]$, $E_2(X_s) = 2\sqrt{J_1^2 + (J_2 - 2J_2')(J_2 - 2J_3) + \omega}$, where $\omega = J_1'(J_e - J_2) - J_1(J_1' + 2J_e - 2J_2)$, and $E_4(X_s) = 2[-J_1 + \sqrt{(J_e - J_3' - J_1)(J_1' + J_e - J_3' - J_1)}]$, which also defines the spin-wave bandwidth. Another important experimentally measurable quantity is the spin-wave velocity at low energy, which is given by

$$v_s = \sqrt{\frac{5}{2}}\sqrt{\frac{\{J_1[J_1' + 2(J_2' + J_3 - J_3')] + J_1'(J_2 - J_2' - J_3 + J_3') + 2[J_2(J_2' + J_3 - J_3') + 2J_3(J_3' - J_2')]\}[J_1' + 2(J_2' + J_3)]}{J_1 - J_1' + J_2 - J_2' - J_3 + J_3'}}. \quad (12)$$

We calculate spin-wave spectra and related features for three different parameter sets. We first adopt the parameters $J_1 = (J_{1a} + J_{1b})/2 = -30$ meV, $J_2 = 20$ meV, and $J_3 = 9$ meV. Due to lattice distortion that draws the four spins in each new unit cell closer, the primed parameters can be reduced from unprimed ones by the presence of iron vacancies: $J_1' = -10$ meV, $J_2' = 20$ meV, and $J_3' = 0$ meV because of the vacancy along the exchange pathway. For these parameters the spin-wave spectra have a finite gap $\Delta_{12} = 10.2$ meV between the first and the second branches and a larger gap $\Delta_{34} = 86.2$ meV between the third and fourth branches. The full bandwidth is $W = 167.5$ meV. The first branch starts from zero energy at Γ and M_s and reaches maximum at X_s; the second and third branches start from minimum at $(3\pi/10,\pi/10)$ and its three C_4 equivalents and reach maximum at $(0.45\pi,0.12\pi)$. The fourth branch starts from $E_4(\Gamma)$ at Γ and M_s to $E_4(X_s)$ at X_s. The ordered moment correction from the spin wave is $\delta m = 0.095$. See Figs. 4(a) and 4(b) for details.

In choosing the second parameter set, we consider a purely magnetic model without lattice distortion. Therefore we take $J_1' = J_1$, $J_2' = J_2$. However, one still has $J_3 \gg J_3' \sim 0$ because of the vacancy along the exchange path for J_3'. For this parameter set, there is no gap between the first and second branches, but the gap between the third and fourth branch remains finite. The full bandwidth in this case is $W = 142.7$ meV. The first three branches start from zero energy at Γ and M_s and reach maximum at $(3\pi/10,\pi/10)$ and its three C_4 equivalents. The fourth branch's minimum and maximum appear at the same points as in the first parameter set. The ordered moment correction from the spin wave is $\delta m = 0.197$. See Figs. 4(c) and 4(d) for details.

In FeTe, we found that the third neighbor exchange J_3 is needed to explain both low- and high-energy regions of dynamic spin susceptibility observed in the neutron experiment, while a parameter fit without J_3 significantly underestimates the spin-wave bandwidth. J_3 is also important in the current system to stabilize the 245 state. For comparison, we adopt the parameters we used to fit the FeTe system without J_3 (see supplementary materials in Ref. 26): $(J_1, J_1', J_2, J_2', J_3, J_3') = (-12,-4,9,9,0,0)$ meV. The spin-wave correction to the moment in this case is $\delta m = 0.43$, indicating much stronger spin fluctuation.

The dynamic local susceptibility is shown in Fig. 5. Note that around zero energy the dynamic factor should drop to zero in a three-dimensional system but converge to a finite value in our two-dimensional system. If we include a small J_z in the beginning, we can make the curve drop to zero at zero energy; however, the dynamic factor at $\omega \gg J_z$ is unaffected. See Fig. 5 for the dynamic local susceptibility with all three parameter sets given above.

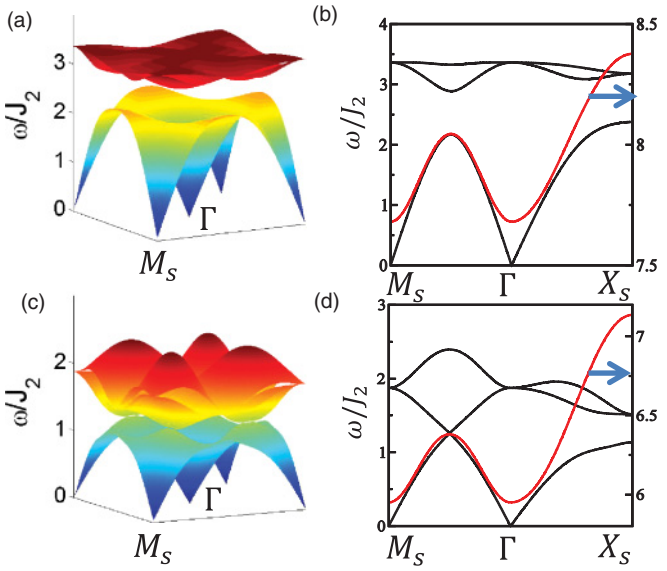

FIG. 4. (Color online) The spin-wave spectra of the lowest three branches (the other one is too high to be drawn in the same plot) using the parameters (a) $(J_1, J_1', J_2, J_2', J_3, J_3') = (-30, -10, 20, 20, 9, 0)$ meV and (c) $(J_1, J_1', J_2, J_2', J_3, J_3') = (-30, -30, 20, 20, 9, 0)$ meV. The corresponding band structures are given in (b) and (d), in which the red dashed lines represent the highest branch and the black solid lines represent the lower three branches. M_s, X_s, and Y_s are high-symmetry points in the BZ that are defined in the text.

To complete our discussion, it is also interesting to check what are the other possible ground-state spin configurations for the same vacancy ordering of the 245 state. In the reasonable parameter space, the following states can be considered: (1) the ferromagnetic state if J_1 and J_1' are large, (2) the AFM2 state in Ref. 38, and (3) the incommensurate phase. The ground-state energy for the first two are easy to calculate: $E_{\rm FM} = 4J_1 + 2J_1' + 2J_2 + 4J_2' + 4J_3 + 2J_3'$ and $E_{\rm AFM2} = -2J_2 - 4\sqrt{(J_2' + J_3)^2 + J_1'^2/4} + J_3'$ (per unit cell in the superlattice). Comparing the energies, we have if $|J_1'| > 2(J_2' + J_3)$ the FM phase wins over the block-AFM phase and if $J_2 > J_3' - J_3 - J_1 + J_2' + J_1'/2 - \sqrt{J_1'^2/4 + (J_2' - J_3)^2}$ AFM2 state has a lower energy than the block-AFM state and thus becomes preferable. Most importantly, an incommensurate (ICM) state is the closest competitor to the block-AFM phase. An analysis of the spin-wave Hamiltonian around the Γ point gives us the phase boundary between the block-AFM state and the ICM as drawn in Fig. 6. The boundary is set by the equation $J_1[J_1' + 2(J_e - J_3')] + J_1'(J_2 - J_e + J_3') + 2[J_2(J_e - J_3') + 2J_3(-J_2' + J_3')] = 0$. We draw Fig. 6(a) for a phase diagram against J_1 and J_1', fixing $J_2 = J_2'$, $J_3 = 9J_2/20$, $J_3' = 0$, and Fig. 6(b) for a phase diagram against J_1 and J_2, fixing $J_1' = J_1$, $J_2' = J_2$ and $J_3' = 0$.

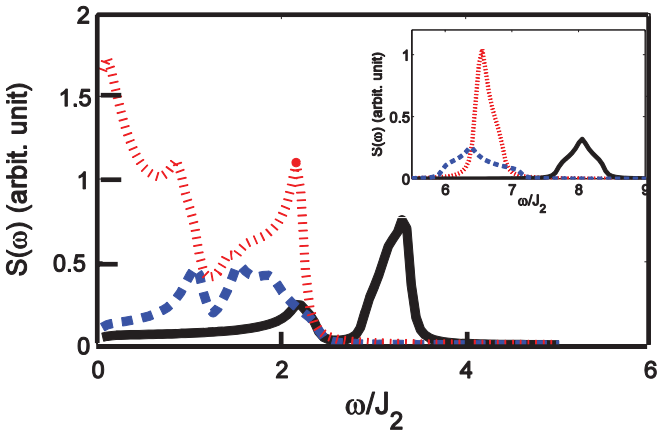

FIG. 5. (Color online) The dynamic factor $S(\omega)$ contributed by the spin wave. The black solid line corresponds to $(J_1, J_1', J_2, J_2', J_3, J_3') = (-30, -10, 20, 20, 9, 0)$ meV; the blue dashed line corresponds to $(J_1, J_1', J_2, J_2', J_3, J_3') = (-30, -30, 20, 20, 9, 0)$ meV; and the red dotted line corresponds to $(J_1, J_1', J_2, J_2', J_3, J_3') = (-12, -4, 9, 9, 0, 0)$ meV. The main panel only includes the contribution from the lowest three branches, as the highest branch is too high to be plotted in the same energy range. Inset: the contribution by the fourth and highest branch.

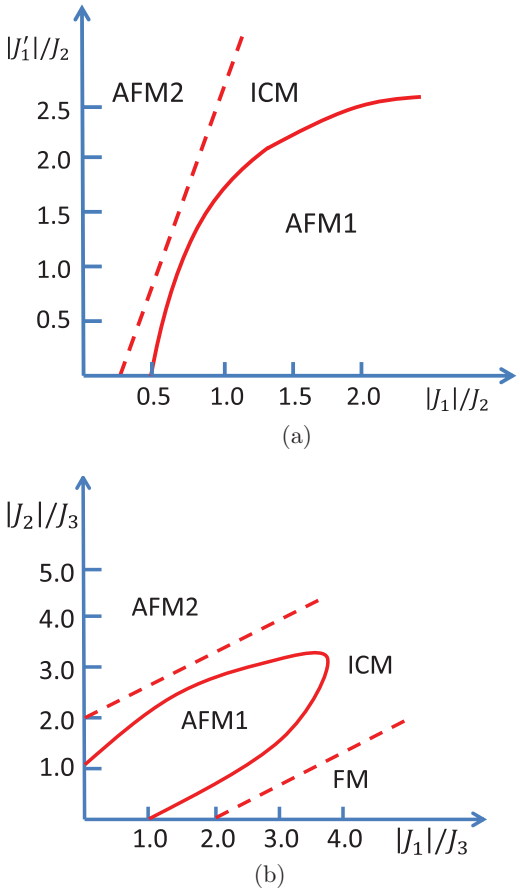

FIG. 6. (Color online) The phase diagrams against (a) J_1 and J_1' taking $J_3 = 9/20 J_2$ and $J_3' = 0$ and (b) J_1 and J_2 taking $J_1' = J_1$, $J_2' = J_2$, and $J_3' = 0$. Solid lines mark second-order transitions calculated from the spin wave, and dotted lines mark possible first-order transitions. FM is the ferromagnet, AFM1 is the block spin, and AFM2 is the commensurate state plotted in Fig. 2(b) of Ref. 38.

Comparing the energies, we have if $|J_1'| > 2(J_2' + J_3)$ the FM phase wins over the block-AFM phase and if $J_2 > J_3' - J_3 - J_1 + J_2' + J_1'/2 - \sqrt{J_1'^2/4 + (J_2' - J_3)^2}$ AFM2 state has a lower energy than the block-AFM state and thus becomes preferable. Most importantly, an incommensurate (ICM) state is the closest competitor to the block-AFM phase. An analysis of the spin-wave Hamiltonian around the Γ point gives us the phase boundary between the block-AFM state and the ICM as drawn in Fig. 6. The boundary is set by the equation $J_1[J_1' + 2(J_e - J_3')] + J_1'(J_2 - J_e + J_3') + 2[J_2(J_e - J_3') + 2J_3(-J_2' + J_3')] = 0$. We draw Fig. 6(a) for a phase diagram against J_1 and J_1', fixing $J_2 = J_2'$, $J_3 = 9J_2/20$, $J_3' = 0$, and Fig. 6(b) for a phase diagram against J_1 and J_2, fixing $J_1' = J_1$, $J_2' = J_2$ and $J_3' = 0$.

After finishing the first version of the paper, three of us collaborated on an experimental work[35] and verified that the case described by the first parameter set is qualitatively consistent with the dynamic spin susceptibility measurement in $Rb_{0.8}Fe_{1.58}Se_2$. A careful fitting was carried out and an improved set of parameters was obtained in that work.

IV. DISCUSSION

We have shown that the 245 vacancy pattern can be naturally obtained through comparing the magnetic energy saving in a strongly frustrated magnetic J_1-J_2-J_3 model. It is necessary to address a few limitations in the model we used and compare our results with other works that have studied the 245 state. First, in our above analysis, we only consider the magnetic energy and ignore other possible energy sources. In real materials, it is possible that other energy sources may make a significant contribution as well. For example, creating a dimer of two vacancies may cost a higher or lower energy than having two individual vacancies. Therefore, comparing a dimer vacancy pattern to a nondimer pattern requires further careful consideration. The LDA calculation may help to address it.[29] Second, we ignore lattice-magnetic coupling, which could be strong in these materials. A lattice distortion that breaks the same lattice symmetry as the magnetic pattern should naturally take place above or at the magnetic transition temperature, similar to what has been observed in iron pnictides.[17] Third, LDA + U calculations have captured the correct magnetic ground state in the 245 vacancy pattern and have extracted the values of magnetic exchange couplings.[7] However, the extracted values are not consistent with our picture. In their results, the NNN exchange couplings J_2' and J_2 are very different and there is no J_3. We expect that J_2 and J_2' should be not drastically different and J_3 should be non-negligible. Similar inconsistency between LDA results and experimental results on the values of magnetic exchange couplings also exists in FeTe.[26,30] Such an inconsistency may stem from the fact that LDA calculations essentially are mean-field solutions. The exchange couplings extracted from LDA calculations depend on designed magnetic structures' energies, which are compared, as well as on the strength of electron-electron correlation in LDA+U. Finally, the NN exchange coupling is strongly FM, which contributes the largest part of the energy in the 245 phase. This strong FM coupling leads to a high magnetic transition temperature observed in the 245 phase. It is interesting to note that the 245 pattern has also been obtained in the one-band $t - J - V$ model,[31] which is driven by magnetic energy saving in proper parameter regions.

Our results also have important implications on superconductivity in these materials. The ferromagnetic coupling does not contribute to any spin singlet pairing in a superconducting (SC) state. Therefore, although the NN FM coupling can cause a high magnetic transition temperature in the 245 state, the SC transition temperature is not expected to scale with the magnetic transition temperature because the SC transition temperature is determined by the strength of the AFM couplings. The SC pairing is mainly determined by the AFM J_2.[32] Since the SC transition temperatures for both iron pnictides and iron chalcogenides are similar, the J_2 value is expected to be similar as well.[33,34] The existence or absence of J_3 differentiates iron chalcogenides from iron pnictides. J_3 leads different magnetic orders in iron chalcogenides. The effect of J_3 in the superconducting state should also be interesting. In fact, J_3 can enhance the s-wave pairing significantly when electron pockets dominate over hole pockets. Finally, as the 245 pattern is very strong in magnetism, we do not think this state can coexist with the superconducting phase.

We have noted relevant spin-wave calculations done by other authors[36,37] and a study of the magnetic phase diagram of the 245 vacancy-ordered phase.[38] The model used in their works is the J_1-J_2-J_1'-J_2' model. Formally speaking, our model comprises this model by setting $J_3 = J_3' = 0$, and the parameters chosen in those works are supported by first-principle calculations while our parameters are chosen based on a previous fit to the experimental data from an inelastic neutron scattering on FeTe.[26] In the spin-wave calculations in Refs. 36 and 37, the first three branches touch each other in dispersion, while our dispersion (with the first parameter set) has one distinct magnon branch and two optical branches separated from the magnon branch by a finite gap. Additionally, the band top of the spin-wave dispersion in Ref. 36 is about one half of our band top. Reference 38 has a thorough discussion of the magnetic phase diagram with a wide range of parameters. In the parameter region of $J_1 < J_1' < 0$ and $J_3 = J_3' = 0$, we obtain a consistent phase diagram with Fig. 2(b) of their work. Reference 38 also calculates the phase boundary between the incommensurate and the block-spin phases, but we are the first to give an analytic expression of this boundary in terms of the parameters. In the spin-wave calculation, we have also obtained the closed-form expression of the spin-wave velocity, a quantity that may be extracted with some accuracy in inelastic neutron-scattering experiments.

V. CONCLUSION

In summary, the J_1-J_2-J_3 model provides a natural and unified understanding for magnetism and vacancy ordering in iron chalcogenides. The 245 vacancy pattern reduces the magnetic frustration and achieves the maximal magnetic energy saving. The reduction of frustration increases the ordered magnetic moment and strongly increases the magnetic transition temperature.

ACKNOWLEDGMENTS

J. P. thanks S. A. Kivelson, Hong Ding, Donglai Feng, and X. H. Chen for useful discussion.

*Current address: Department of Physics, Princeton University, Princeton, NJ 08544.

[1] J. Guo, S. Jin, G. Wang, S. Wang, K. Zhu, T. Zhou, M. He, and X. Chen, Phys. Rev. B **82**, 180520 (2010).

[2] M. Fang, H.-D. Wang, C.-H. Dong, Z.-J. Li, C.-M. Feng, J. Chen, and H. Q. Yuan, Europhys. Lett. **94**, 27009 (2011).

[3] R. H. Liu, X. G. Luo, M. Zhang, A. F. Wang, J. J. Ying, X. F. Wang, X. J. Yan, Z. J. Xiang, P. Cheng, G. J. Ye, Z. Y. Li, and X. H. Chen, Europhys. Lett. **94**, 27008 (2011).

[4] Y. Zhang, L. X. Yang, M. Xu, Z. R. Ye, F. Chen, C. He, H. C. Xu, J. Jiang, B. P. Xie, J. J. Ying, X. F. Wang, X. H. Chen, J. P. Hu, M. Matsunami, S. Kimura, and D. L. Feng, Nat. Mater. **10**, 273 (2010).

[5] X. Wang, T. Qian, P. Richard, P. Zhang, J. Dong, H.-D. Wang, C.-H. Dong, M. H. Fang, and H. Ding, Europhys. Lett. **93**, 57001 (2011).

[6]D. Mou, S. Liu, X. Jia, J. He, Y. Peng, L. Zhao, L. Yu, G. Liu, S. He, X. Dong, J. Zhang, H. Wang, C. Dong, M. Fang, X. Wang, Q. Peng, Z. Wang, S. Zhang, F. Yang, Z. Xu, C. Chen, and X. J. Zhou, Phys. Rev. Lett. **106**, 107001 (2011).
[7]C. Cao and J. Dai, Phys. Rev. Lett. **107**, 056401 (2011).
[8]L. Zhang and D. J. Singh, Phys. Rev. B **79**, 094528 (2009).
[9]X. W. Yan, M. Gao, Z. Y. Lu, and T. Xiang, Phys. Rev. B **84**, 054502 (2011).
[10]W. Bao, Q. Huang, G. F. Chen, M. A. Green, D. M. Wang, J. B. He, X. Q. Wang, and Y. Qiu, Chin. Phys. Lett. **28**, 086104 (2011).
[11]W. Bao, G. N. Li, Q. Huang, G. F. Chen, J. B. He, M. A. Green, Y. Qiu, D. M. Wang, and J. L. Luo, e-print arXiv:1102.3674v1 (2011).
[12]J. Bacsa, A. Y. Ganin, Y. Takabayashi, K. E. Christensen, K. Prassides, M. J. Rosseinsky, and J. B. Claridge, Chem. Sci. **2**, 1054 (2011).
[13]V. Y. Pomjakushin, D. V. Sheptyakov, E. V. Pomjakushina, A. Krzton-Maziopa, K. Conder, D. Chernyshov, V. Svitlyk, and Z. Shermadini, Phys. Rev. B **83**, 144410 (2011).
[14]Z. Wang, Y. J. Song, H. L. Shi, Z. W. Wang, Z. Chen, H. F. Tian, G. F. Chen, J. G. Guo, H. X. Yang, and J. Q. Li, Phys. Rev. B **83**, 140505(R) (2011).
[15]P. Zavalij, W. Bao, X. F. Wang, J. J. Ying, X. H. Chen, D. M. Wang, J. B. He, X. Q. Wang, G. F. Chen, P.-Y. Hsieh, Q. Huang, and M. A. Green, Phys. Rev. B **83**, 132509 (2011).
[16]A. M. Zhang, K. Liu, J. H. Xiao, J. B. He, D. M. Wang, G. F. Chen, B. Normand, and Q. M. Zhang, Phys. Rev. B **85**, 024518 (2012).
[17]Clarina de la Cruz, Q. Huang, J. W. Lynn, Jiying Li, W. Ratcliff II, J. L. Zarestky, H. A. Mook, G. F. Chen, J. L. Luo, N. L. Wang, and P. Dai, Nature (London) **453**, 899 (2008).
[18]Q. Si and E. Abrahams, Phys. Rev. Lett. **101**, 076401 (2008).
[19]C. Fang, H. Yao, W.-F. Tsai, J. P. Hu, and S. A. Kivelson, Phys. Rev. B **77**, 224509 (2008).
[20]W. Bao, Y. Qiu, Q. Huang, M. A. Green, P. Zajdel, M. R. Fitzsimmons, M. Zhernenkov, S. Chang, M. Fang, B. Qian, E. K. Vehstedt, J. Yang, H. M. Pham, L. Spinu, and Z. Q. Mao, Phys. Rev. Lett. **102**, 247001 (2009).
[21]S. Li, C. de la Cruz, Q. Huang, Y. Chen, J. W. Lynn, J. Hu, Y.-L. Huang, F.-C. Hsu, K.-W. Yeh, M.-K. Wu, and P. Dai, Phys. Rev. B **79**, 054503 (2009).
[22]F.-C. Hsu, J.-Y. Luo, K.-W. Yeh, T.-K. Chen, T.-W. Huang, P. M. Wu, Y.-C. Lee, Y.-L. Huang, Y.-Y. Chu, D.-C. Yan, and M.-K. Wu, Proc. Natl. Acad. Sci. **105**, 14262 (2008).
[23]Y. Mizuguchi, F. Tomioka, S. Tsuda, T. Yamaguchi, and Y. Takano, Appl. Phys. Lett. **93**, 152505 (2008).
[24]F. Ma, W. Ji, J. Hu, Z.-Y. Lu, and T. Xiang, Phys. Rev. Lett. **102**, 177003 (2009).
[25]C. Fang, B. A. Bernevig, and J. Hu, Europhys. Lett. **86**, 67005 (2009).
[26]O. J. Lipscombe, G. F. Chen, C. Fang, T. G. Perring, D. L. Abernathy, A. D. Christianson, T. Egami, N. Wang, J. Hu, and P. Dai, Phys. Rev. Lett. **106**, 057004 (2011).
[27]X. Li *et al*. (unpublished).
[28]V. J. Emergy, S. A. Kivelson, and J. M. Tranquada, Proc. Natl. Acad. Sci. **96**, 8814 (1999).
[29]X. W. Yan, M. Gao, Z. Y. Lu, and T. Xiang, Phys. Rev. B **83**, 233205 (2011).
[30]K. W. Lee, V. Pardo, and W. E. Pickett, Phys. Rev. B **78**, 174502 (2008).
[31]S. A. Kivelson, V. J. Emery, and H. Q. Lin, Phys. Rev. B **42**, 6523 (1990).
[32]K. Seo, B. A. Bernevig, and J. Hu, Phys. Rev. Lett. **101**, 206404 (2008).
[33]J. Zhao, D. T. Adroja, D.-X. Yao, R. Bewley, S. Li, X. F. Wang, G. Wu, X. H. Chen, J. Hu, and P. Dai, Nature Physics **5**, 555 (2009).
[34]J. Zhao, D.-X. Yao, S. Li, T. Hong, Y. Chen, S. Chang, W. Ratcliff, J. W. Lynn, H. A. Mook, G. F. Chen, J. L. Luo, N. L. Wang, E. W. Carlson, J. Hu, and P. Dai, Phys. Rev. Lett. **101**, 167203 (2008).
[35]M. Wang, C. Fang, D.-X. Yao, G. Tan, L. W. Harriger, Y. Song, T. Netherton, C. Zhang, M. Wang, M. B. Stone, W. Tian, J. Hu, and P. Dai, Nature Communications **2**, 580 (2011).
[36]Y.-Z. You, H. Yao, and D.-H. Lee, Phys. Rev. B **84**, 020406 (2011).
[37]F. Lu and X. Dai, Chin. Phys. B **21**, 027502 (2012).
[38]R. Yu, P. Goswami, and Q. Si, Phys. Rev. B **84**, 094451 (2011).